Chapter V

Antimicrobial attributes of different nanostructured WS_2 and MoS_2 systems against multiple pathogens

"The beautiful thing about learning is nobody can take it away from you"

- B.B.King

5.1 Introduction

Transition metal dichalcogenides (TMDCs) have achieved several advances in various applications such as photosensing [1,2,3], bio and chemical sensing [4-7], future electronic and valleytronic devices [8-11], catalysis [5, 12, 13], wastewater treatment, toxic gas adsorption and removal [14] etc. Nevertheless, research on TMDCs for biomedical applications is still in its infancy. It is not even earlier than the last two decades when researchers have just started investigating the cytotoxicity of these materials [15-17]. Interestingly, inorganic fullerene-type and few layer structures of WS_2 and MoS_2 have attracted much attention owing to their low cytotoxicity and genotoxicity, as evaluated by different biocompatibility tests [18].

These findings have prompted researchers to investigate antipathogenic activities of these materials. Although limited, several studies have reported interesting results. WS_2 nanosheets synthesized by the hydrothermal method were found to be responsible for bacterial death, with a death rate as high as 99.97 % against *Staphylococcus epidermidis* (*S. epidermidis*). WS_2 nanosheets have also performed well against *Escherichia coli (E. coli)*, *Salmonella typhimurium (S. typhimurium)*, and *Bacillus subtilis (B. subtilis)* at a concentration of 250 μg mL^{-1}. The method used there was the colony counting method [19]. In addition, the antibacterial activity of WS_2 against gram-negative *E. coli* and gram-positive *Staphylococcus aureus (S. aureus)* was evaluated using colony-forming unit studies. Almost 0% viability of the bacterial cultures was observed at a concentration of 200 μg mL^{-1} [20]. The activity of WS_2 and the WS_2/ZnO nanohybrid against *Candida albicans (C. albicans)* was investigated using the disc diffusion method at a concentration of 300 μg mL^{-1}. This led to the inhibition of fungal growth by up to 74% and 91%, respectively [21]. MoS_2 nanosheets synthesized through Li-intercalation showed a loss of *E.coli* viability of 91.8% ± 1.4% at a concentration of 80 μg mL^{-1}. The fact that MoS_2 nanosheets outperformed their bulk counterparts implies the contribution of the high specific surface area and high conductivity of the exfoliated sheets to the destruction of bacterial cells [22]. Furthermore, Li-intercalated, and ligand-functionalized MoS_2 nanosheets were applied against *S. aureus* and *P. aeruginosa*, revealing that exfoliated

MoS_2 with positive charges is more effective in inducing the bactericidal effect [23]. Likewise, 20 μg mL^{-1} of MoS_2 nanosheets exfoliated through solvo-sonication showed antibacterial activity against *Salmonella* and wild-type *S. typhimurium* [24].

As discussed, in recent reports, TMDCs nanosheets have been functionalized with ligands, doped with other material atoms, or blended into composites to obtain enhanced antipathogenic activities. However, the non-functionalized WS_2 and MoS_2 nanosheets also showed significant antibacterial activity against pathogens. Nevertheless, in most reports, only a few pathogens were simultaneously targeted by the materials. Therefore, it is necessary to evaluate the antimicrobial properties of the non-functionalized forms of these materials against multiple pathogens.

Accordingly, an experiment has been carried out in order to investigate the polyvalent antipathogenic activity of WS_2 and MoS_2 nanosheets against six different pathogens, including five bacterial cultures and one fungal culture, and compared the results for WS_2 and MoS_2 nanosheets. Again, we have employed four different methods of synthesis of WS_2 and MoS_2 in order to determine the key aspects responsible for showing antipathogenic activities. The antipathogenic activity was evaluated using agar well diffusion method. For all the experiments, liquid-dispersed specimens of WS_2 and MoS_2 were used.

5.2 Experimental details

5.2.1 Agar well diffusion assay

Agar well diffusion method is one of the popular antibacterial assays. The processes involved in this assay are described below.

5.2.1.1 Preparation of lysogeny broth (LB) and potato dextrose broth (PDB) media

In order to prepare lysogeny broth (LB, Miller) media, 12.5 g premixed LB(Miller) powder (HiMedia) was dissolved in 500 ml of distilled water. LB (Miller) powder was composed of tryptone, yeast extract and sodium chloride (NaCl) mixed in 2:1:2 ratio. For preparation of LB agar media, bacteriological agar (HiMedia) was added to LB broth to a final concentration of 1.8% (w/v). The mixture was heated in a microwave for 1-2 min for dissolving the agar and then, the culture media was sterilized in an autoclave at 15 psi, 121

°C for 20 min. For preparation of PDB media, 12 g of potato dextrose broth powder (granulated, HiMedia) was dissolved in 500 ml of distilled water. For the preparation of

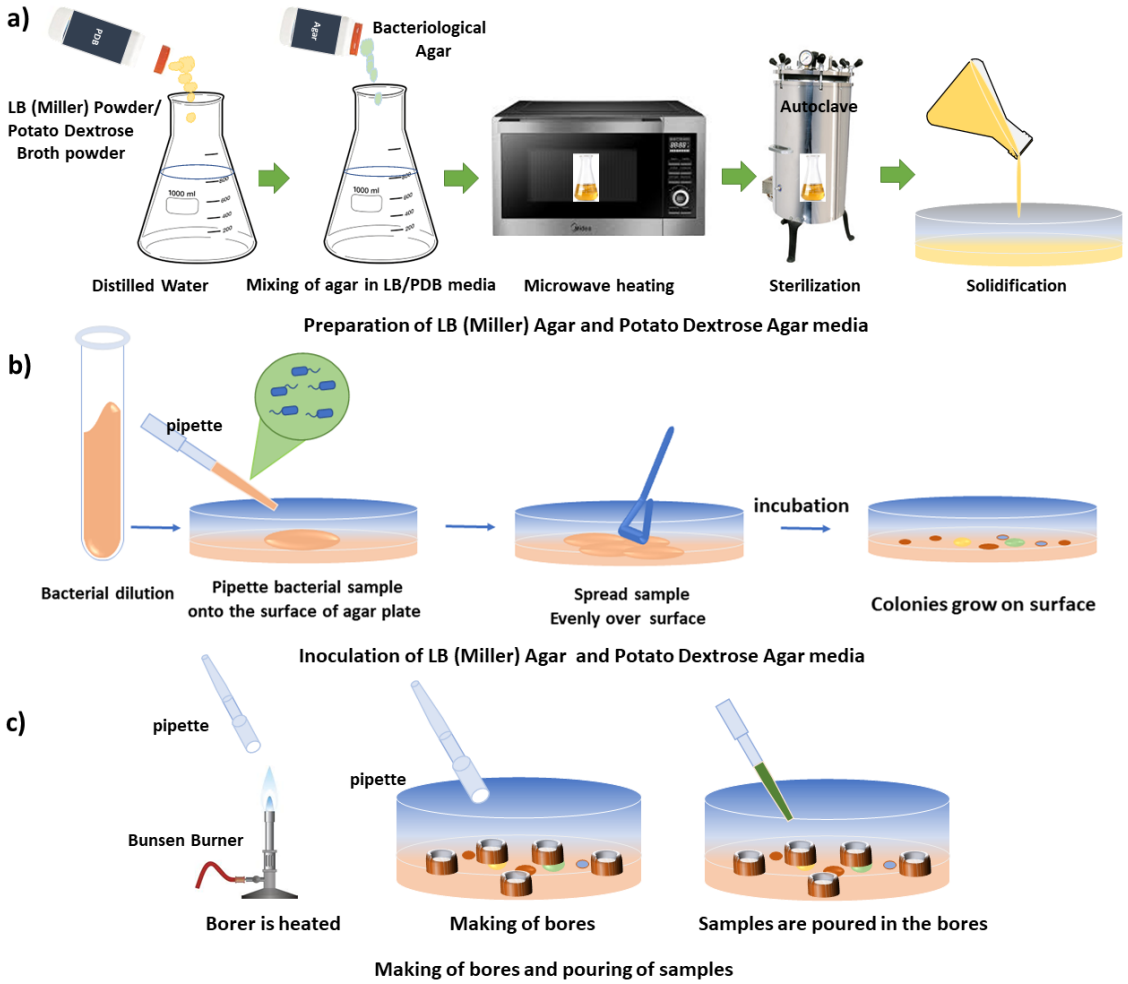

Fig.5.1. **(a)** Preparation of LB(Miller) agar and PDB agar media **(b)** Inoculation of LB(Miller) agar and potato dextrose agar media **(c)** Making of bores and pouring of samples.

potato dextrose agar media, bacteriological agar was added to PDB to a final concentration of 2% (w/v). The mixture was heated in a microwave for 1-2 min for dissolving the agar and then the culture media was sterilized in an autoclave at 15 psi, 121 °C for 20 min. After autoclaving, the agar media (25 ml) was poured onto each petri dish under sterile conditions (in a laminar air flow hood) and allowed to solidify. Finally, the petri dishes containing solidified agar media was used for antimicrobial assay. The schematics of the preparation of LB (Miller) and PDB media is shown in **Fig 5.1(a)**.

5.2.1.2 Inoculation of LB (Miller) agar and potato dextrose agar media and making of wells

Inoculation of different agar media is done by using spread method. 100 µL of bacterial or fungal inoculum is spread onto the solidified agar surface. Thus, bacterial cultures of *Mycobacterium smegmatis (MS), Staphylococcus aureus (SA), Bacillus cereus (BC), Pseudomonas aeruginosa (PA), Yersinia pestis (YP), Escherichia. coli (EC)* and a fungal culture of *Candida albicans (CA)* were grown overnight in LB (Miller) and PDB, respectively. The process of inoculation is illustrated in **Fig. 5.1(b)**.

Table 5.1. Name and MTCC of the bacterial and fungal cultures.

S. No.	**Name**	**MTCC No.**
1	*Mycobacterium smegmatis (MS)*	MTCC 14468
2	*Staphylococcus aureus (SA)*	MTCC 3160
3	*Bacillus cereus (BC)*	MTCC 430
4	*Pseudomonas aeruginosa (PA)*	MTCC 2297
5	*Yersinia pestis (YP)*	NA
6	*Candida albicans (CA)*	MTCC 3017
7	*Escherichia. coli (EC)*	MTCC 40

5.2.1.3 Boring of wells and pouring of TMDC specimens on wells

Wells were bored on the inoculated media using the large opening of a micropipette. 100 µL of specimens were poured into the wells. Gentamicin is an aminoglycoside antibiotic and it has broad spectrum of antibacterial activity [26]. Similarly, Nystatin [27] also has wide spectrum antifungal activity. As such, Gentamicin (2.5 mg mL^{-1}) and Nystatin (5 mg mL^{-1}) were used as positive controls (labelled as P.C.) for bacterial and fungal cultures respectively. The plates were incubated overnight at appropriate temperature (37°C and 28°C for the bacteria and fungi respectively). After incubation (24 h) the plates were evaluated for antimicrobial activity and Zone of Inhibitions (ZOIs) were checked accordingly. The MTCC No. of the bacterial and fungal cultures are listed in **Table 5.1**. **Fig. 5.1** comprises all the processes involved in agar well diffusion method. The processes involved in making of bores and pouring of specimens are shown in **Fig 5.1(c)**

5.2.2 Preparation of WS_2 and MoS_2 nanostructures (Method 1)

WS_2 and MoS_2 flakes (1.6 mg each) were dispersed in 1 mL of the solvent in separate beakers and ultrasonicated in a bath sonicator (Jain Scientific Glass Works, output power:100 W, output frequency:50 Hz). The temperature of the system was maintained at below 30°C. For MoS_2, sonication was performed for 4 h, whereas for WS_2, sonication was performed for 10 h followed by 24 h of rest. After 24 h, the TMDC specimens were centrifuged at 1 krpm for 2 h at 25 °C. After centrifugation, the supernatant was separated from the pellet. Then, 2 mL of the supernatant was retained for characterization, and another portion of the sample was centrifuged for 2 h at 25°C at 1.5 krmp. The supernatant obtained after centrifugation was separated from the pellets, as previously described. This new supernatant (2 mL) was retained for characterization and the remaining portion was centrifuged again for 2 h at 25°C and 2 krpm. This process was continued for higher krpms, such as 2.5, 3, 5 and 7.5 krpm. 2.5 mL of the supernatants after centrifugation at 2 krpm

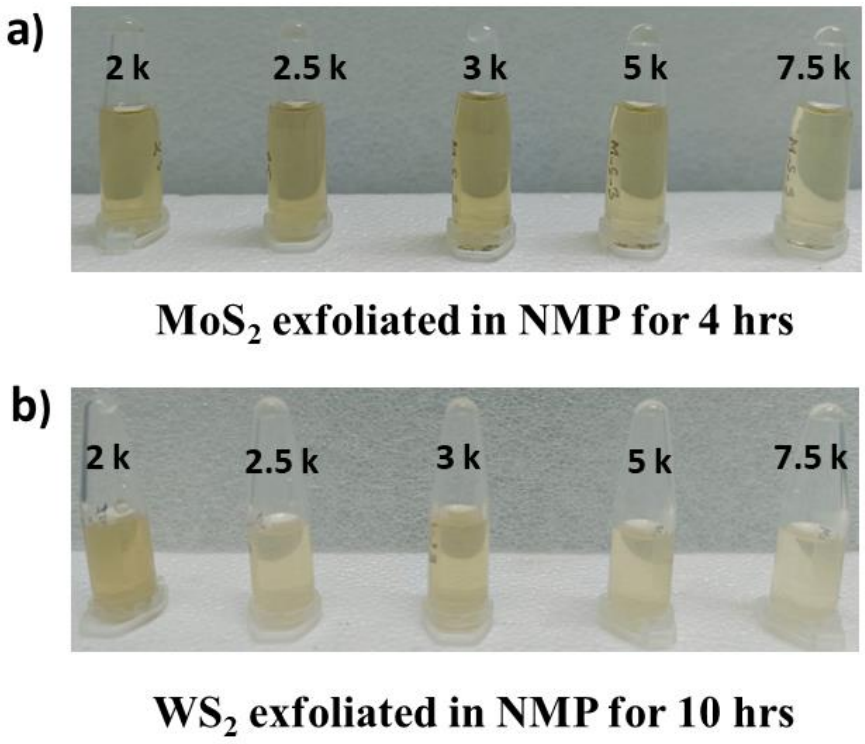

Fig.5.2. (a) MoS_2 specimens exfoliated in NMP for 4 h. **(b)** WS_2 specimens exfoliated in NMP for 10 h. The specimens centrifuged at different rpm viz- 2 krpm, 2.5 krpm, 3 krpm, 5 krpm and 7.5 krpm respectively are labelled as 2 k, 2.5 k, 3 k, 5 k and 7.5 k.

and 7.5 krpm centrifugation processes were kept separately for RPM (rotation per minute)-dependent antibacterial and antifungal assessments of few-layer WS_2 and MoS_2. The method of repeated centrifugation of the supernatant of the specimens at a higher rpm is

known as liquid cascade centrifugation. This idea of the synthesis of a monolayer-enriched dispersion of TMDC nanosheets was borrowed from Backes *et al.* [25]. The specimens obtained after each centrifugation step are shown in **Fig. 5.2.**

5.3 Results (Method 1)

5.3.1 Characterization of synthesized nanostructures

5.3.1.1 X-ray diffraction (XRD) spectroscopy

The XRD spectra of the as-synthesized MoS_2 and WS_2 are presented in **Fig. 5.3(a)** and **Fig. 5.3(b)**, respectively. The diffraction peaks of the synthesized nanostructures corresponded to the hexagonal (*2H*) crystallographic phase of the nanostructures. It is observed that intensity of the diffraction peaks of the exfoliated nanosheets are relatively weaker than that of their bulk counterpart corroborating the exfoliation process [28]. Further details of the XRD peaks are given in **Table AT3**[¥] and **Table AT4**[£].

5.3.1.2 UV-vis Spectroscopy

In **Fig. 5.3(c)** presents the UV-vis spectra of MoS_2 nanosheets. Sharp excitonic peaks at ~ 666 nm, shoulder peaks at ~ 607 nm and ~ 446 nm were observed. These peaks are labelled as A, B, and C, respectively. In the UV spectra of WS_2 (**Fig. 5.3(d)**), a sharp excitonic peak at ~ 633 nm and shoulder peaks at ~ 526 and ~ 458 nm were observed. These three peaks are also labelled as A, B and C respectively. Origin of these peaks are discussed in *section 2.2.5* of *chapter II*.

[¥, £]**Appendix**

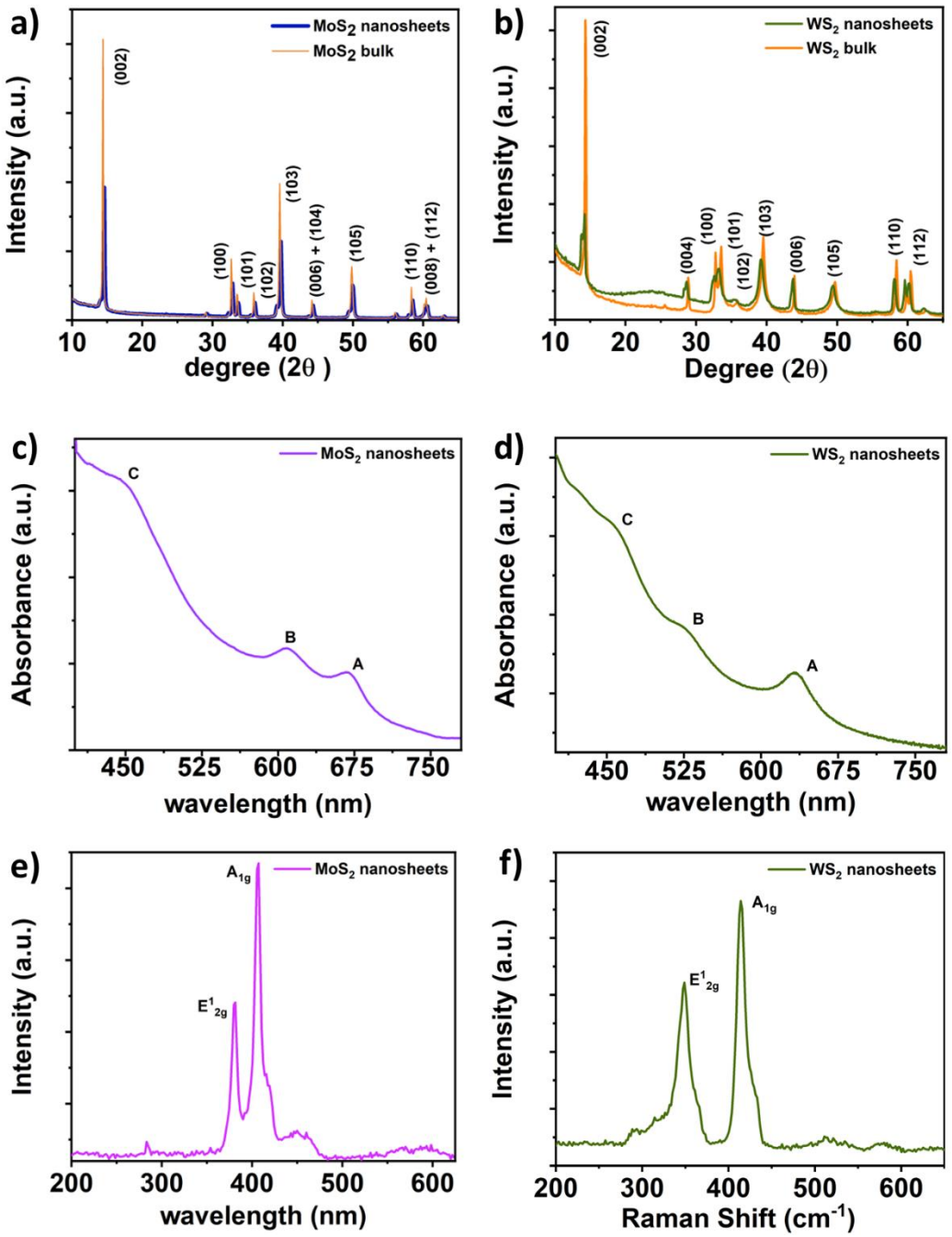

Fig.5.3. X-Ray Diffraction spectra of **(a)** MoS_2 and **(b)** WS_2 bulk and nanosheets; UV-vis spectra of **(c)** MoS_2 and **(d)** WS_2 nanosheets; Raman spectra of **(e)** MoS_2 and **(f)** WS_2 nanosheets.

5.3.1.3 Raman Spectroscopy

Fig. 5.3(e) shows the Raman spectra of exfoliated MoS_2 nanosheets. It exhibits two prominent peaks at ~ 381 cm^{-1} and ~ 407 cm^{-1}, corresponding to E^1_{2g} *(Γ)* and A_{1g} *(Γ)* modes, respectively. **Fig. 5.3(f)** shows the Raman spectra of the exfoliated multilayer WS_2 nanosheets. It exhibits two prominent peaks at ~ 349 cm^{-1} and ~ 414 cm^{-1}, corresponding to the E^1_{2g} *(Γ)* and A_{1g} *(Γ)* modes, respectively. The meaning of these modes is discussed in *section 2.2.4* of *chapter II*.

5.3.1.4 Transmission Electron Microscopy (TEM)

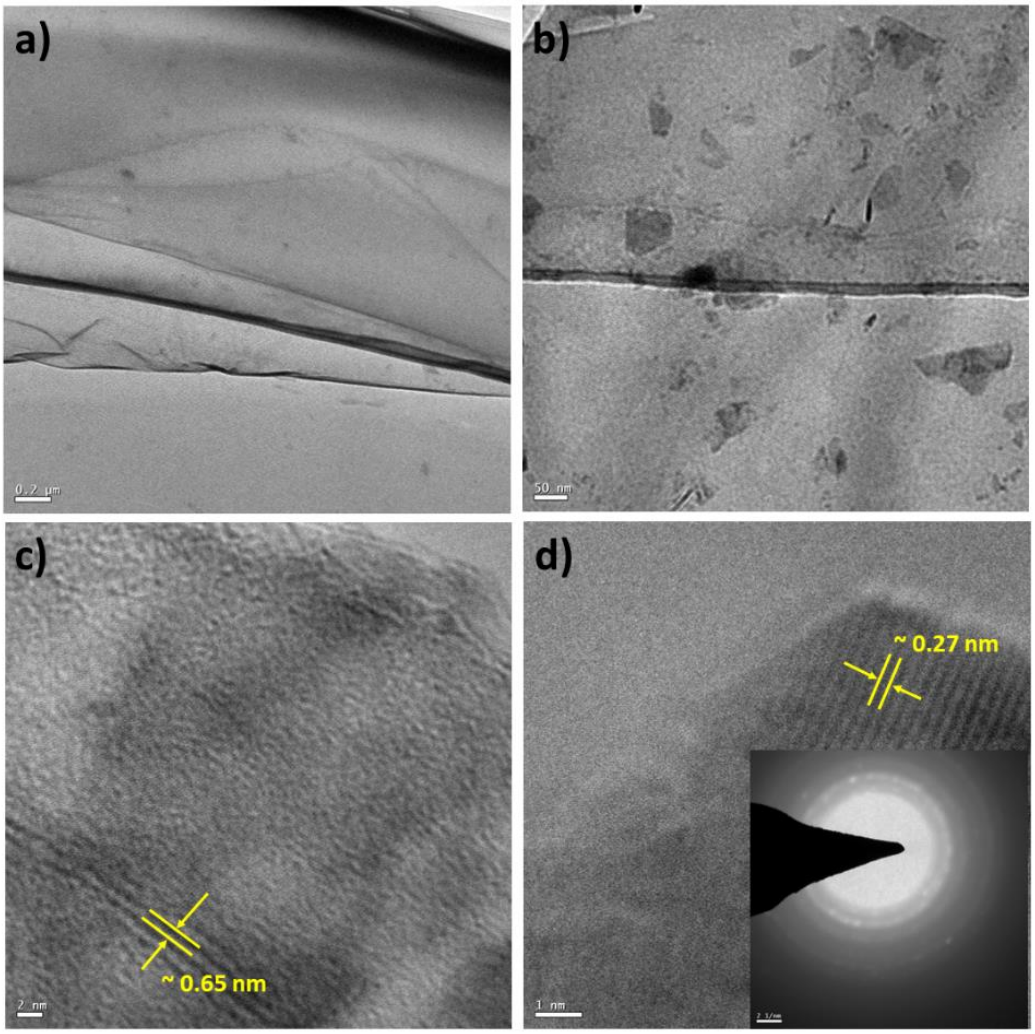

Fig.5.4. TEM micrographs of few-layer MoS_2 nanosheets **(a)** low magnification TEM micrograph (scale bar— 0.2 µm) **(b)** low magnification TEM micrograph (scale bar— 100 nm), SAED in the inset **(c)** TEM micrograph of MoS_2 nanosheets showing interlayer spacing **(d)** TEM micrograph of MoS_2 nanosheets showing lattice fringes, inset shows the SAED pattern**.**

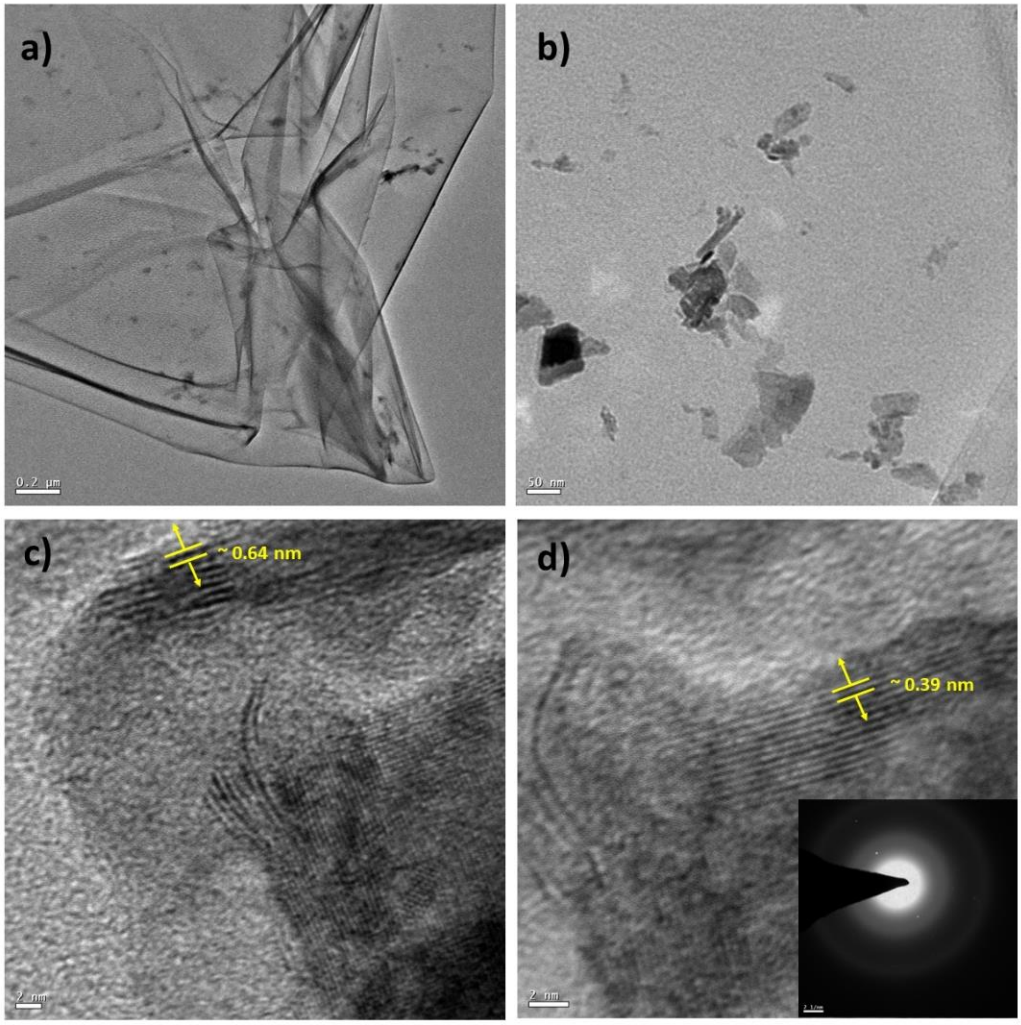

Fig. 5.5 TEM micrographs of few layer WS_2 nanosheets **(a)** low magnification TEM micrograph (scale bar— 0.2 µm) **(b)** low magnification TEM micrograph (scale bar— 50 nm) **(c)** TEM micrograph of WS_2 nanosheets showing interlayer spacing **(d)** TEM micrograph of WS_2 nanosheets showing lattice fringes (inset shows the SAED pattern)

The obtained MoS_2 nanosheets were further characterized using TEM to elucidate their structural properties. As shown in **Fig. 5.4(a)**, the as-synthesized MoS_2 was in the form of layers (scale bar – 0.2 µm). **Fig. 5.4(b)** shows a magnified image of the MoS_2 nanosheets (scale bar – 100 nm). **Fig 5.4(c)** shows the interlayer distance between the two layers of MoS_2 nanosheets (scale bar – 2 nm). It was found to be 0.65 nm (**Fig. A13[A], Table AT5[₩]**), corresponding to the (002) plane of *2H* MoS_2. In **Fig 5.4(d)**, the high-resolution micrograph of the MoS_2 nanosheets (scale bar – 1 nm) is further analysed to observe the lattice *d*-spacing of ~ 0.27 nm (**Fig. A14[F], Table AT6[€]**). This corresponds to the (100) lattice plane of the hexagonal MoS_2 and is in good agreement with the XRD results. The selected area electron diffraction (SAED) pattern is provided in the inset. The thicknesses

of the nanosheets were in the range of 2–9 nm. In a similar fashion, TEM characterization of the WS_2 nanosheets was performed. **Fig. 5.5(a)** shows the as-synthesized sheet-like structure of WS_2 (scale bar – 0.2 µm). **Fig. 5.5(b)** shows a magnified view of the WS_2 nanostructures (scale bar – 50 nm). **Fig. 5.5(c)** shows a highly resolved micrograph of the WS_2 nanostructures (scale bar – 2 nm). This micrograph was further analysed to obtain the interlayer distance to be ~ 0.64 nm corresponding to (002) plane. **Fig 5.5(d)** shows the high-resolution micrograph of WS_2 nanosheets (scale bar – 2 nm). **Fig 5.5(d)** also shows the SAED pattern in the inset. Analysis shows that the thickness of the nanosheets was ~8 nm (**Fig.A16**[β], **Table AT8**[₱]).

5.3.2 Screening for antimicrobial activity

Photographs of the bacterial and fungal cultures after 24 h of incubation with MoS_2 and WS_2 nanosheets exfoliated in NMP for different durations are shown in **Fig. 5.6** and **5.7**, respectively. Gentamicin (G) was used as the positive control for bacterial cultures *viz.*, *MS*, *SA*, *BC*, *PA*, and *YP*, whereas, Nystatin (N) was used as the positive control for fungal

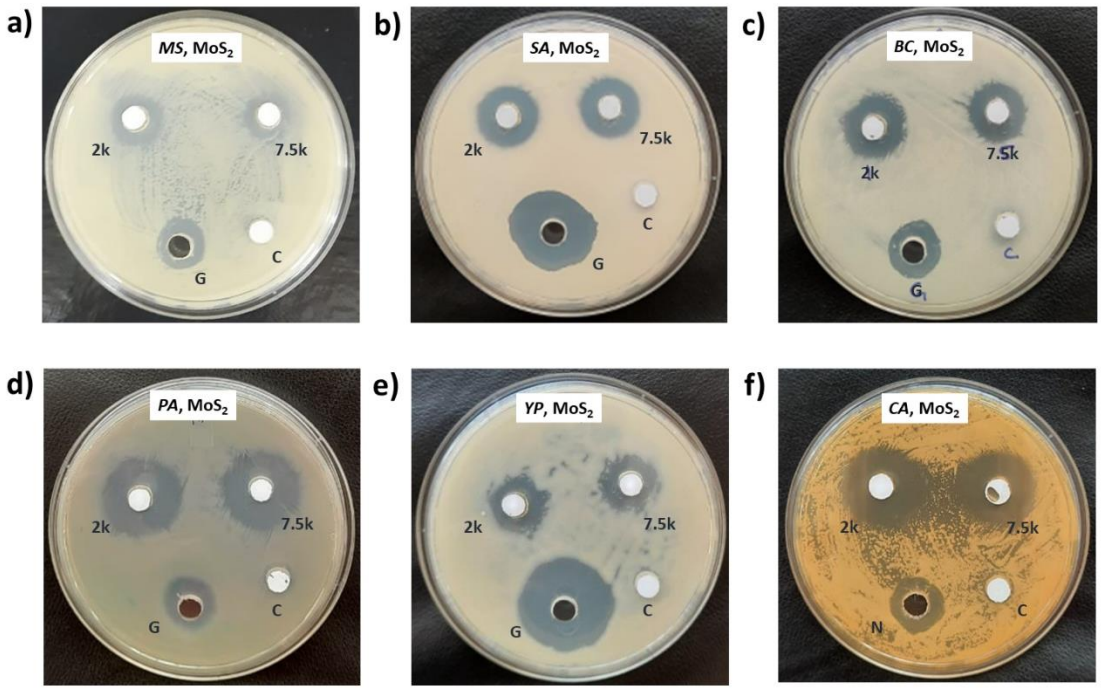

Fig. 5.6. Antimicrobial assessment of MoS_2 exfoliated in NMP for 4 h against **(a)** *Mycobacterium smegmatis (MS)*, **(b)** *Staphylococcus aureus (SA)*, **(c)** *Bacillus cereus (BC)*, **(d)** *Pseudomonas aeruginosa (PA)*, **(e)** *Yersinia pestis (YP)*, and **(f)** a fungal culture of *Candida albicans (CA)*. MoS_2 nanosheets centrifuged at 2 krpm and 7.5 krpm are labelled as 2 k and 7.5 k.

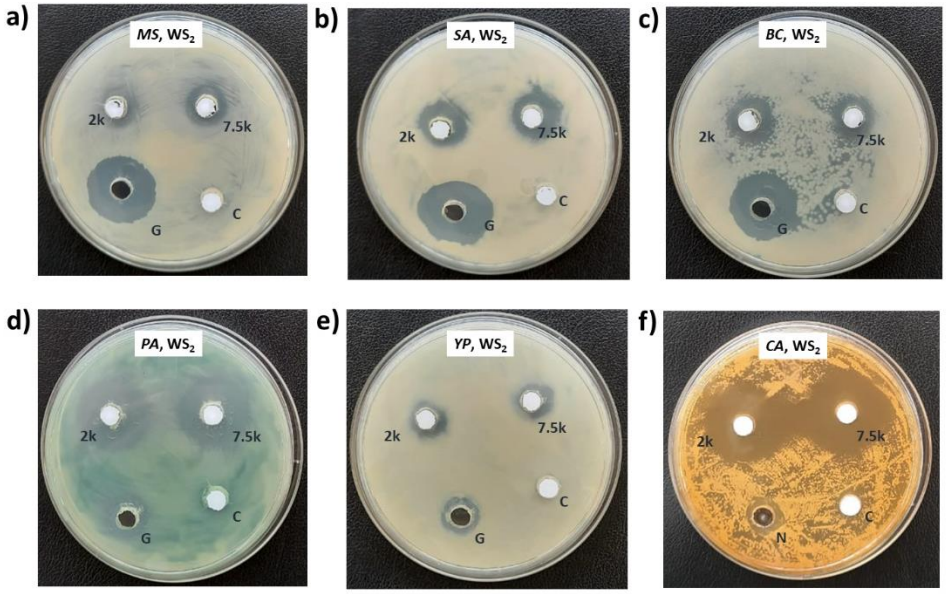

Fig. 5.7. Antimicrobial assessment of WS_2 exfoliated in NMP for 10 h against **(a)** *Mycobacterium smegmatis (MS),* **(b)** *Staphylococcus aureus (SA),* **(c)** *Bacillus cereus (BC),* **(d)** *Pseudomonas aeruginosa (PA),* **(e)** *Yersinia pestis (YP),* and **(f)** a fungal culture of *Candida albicans (CA).* WS_2 nanosheets centrifuged at 2 krpm and 7.5 krpm are labelled as 2 k and 7.5 k.

culture *CA*. WS_2 and MoS_2 nanosheets centrifuged at 2 krmp and 7.5 krpm were labelled as 2 k and 7.5 k. The solvent NMP which was used to disperse the specimens was considered as the carrier control and was labelled as C. **Fig. 5.8** shows the ZOI of MoS_2

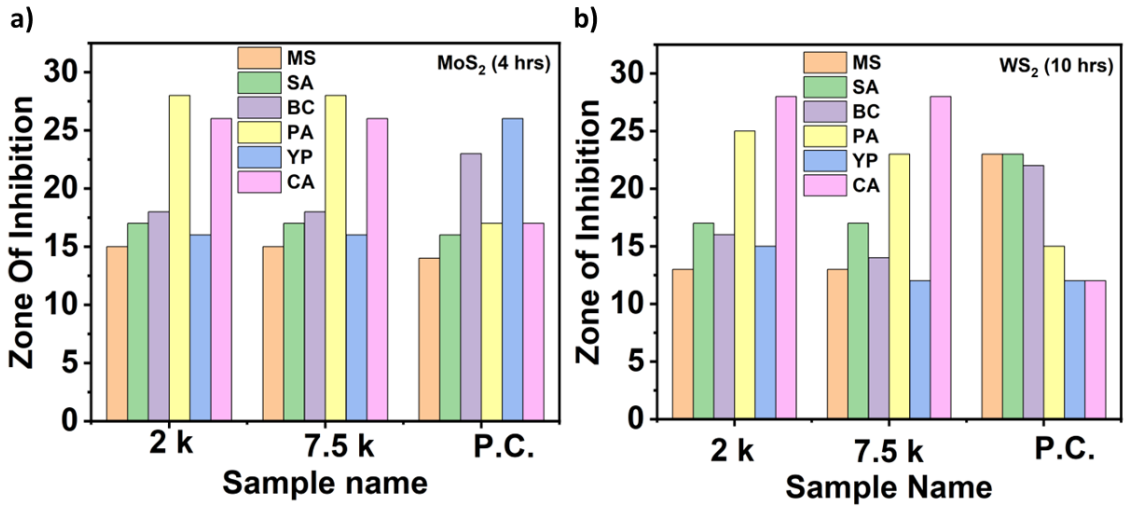

Fig. 5.8. (a) Zone of inhibition (ZOI) of MoS_2 nanosheets (exfoliated in NMP for 4 h) and **(b)** ZOI of WS_2 nanosheets (exfoliated in NMP for 10 h) against *Mycobacterium smegmatis (MS), Staphylococcus aureus (SA), Bacillus cereus (BC), Pseudomonas aeruginosa (PA), Yersinia pestis (YP),* and a fungal culture of *Candida albicans (CA).* WS_2 and MoS_2 nanosheets centrifuged at 2 krpm and 7.5 krpm are labelled as 2 k and 7.5 k. Positive controls are labelled as P.C.

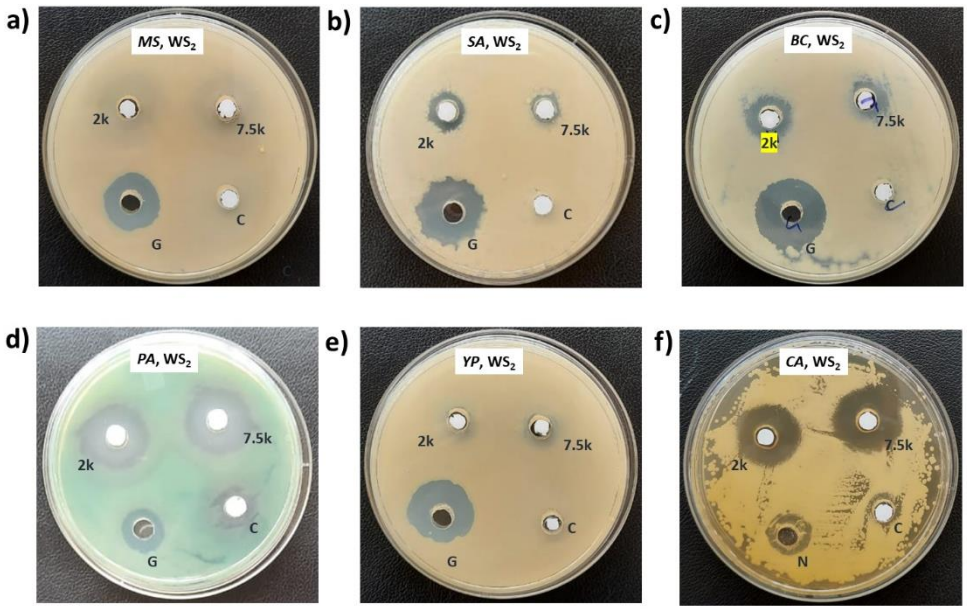

Fig. 5.9. Antibacterial and antimicrobial assessment of WS_2 exfoliated in NMP for 13 h against **(a)** *Mycobacterium smegmatis (MS)* **(b)** *Staphylococcus aureus (SA)* **(c)** *Bacillus cereus (BC)* **(d)** *Pseudomonas aeruginosa (PA)* **(e)** *Yersinia pestis (YP)*, and **(f)** a fungal culture of *Candida albicans (CA)*. WS_2 nanosheets centrifuged at 2 krpm and 7.5 krpm are labelled as 2 k and 7.5 k.

and WS_2 nanosheets against bacterial and fungal cultures. **Fig. 5.8** suggests that MoS_2 and WS_2 performed better than the positive controls in the case of *PA* and *CA*. On the other hand, the positive controls performed better than these specimens against *BC*. To analyse the susceptibility pattern of pathogens towards the TMDC specimens, the range of different susceptibility levels are enlisted in **Table 5.2** [29]. On the basis of the categorization done in **Table 5.2, Table 5.3** summarizes the susceptibility pattern of pathogens towards the TMDC nanostructures. In case of few-layer MoS_2 nanostructures, all the pathogens were susceptible, however in case of WS_2, all the pathogens except *MS* were susceptible. *MS* showed intermediate susceptibility towards WS_2 specimens. It was observed that few-layer MoS_2 nanostructures can perform better as antipathogenic agents than few-layer WS_2 nanostructures, even at concentrations as low as three times (**Table 5.3**) than that of WS_2. Again, it was already mentioned that it took at least 6 h more to prepare few-layer WS_2 nanostructures than MoS_2 nanostructures. Therefore, it may be concluded that MoS_2 is more effective as antipathogenic agent than WS_2.

In addition to the synthesis method described above, several other methods have been applied to determine the key parameters affecting the antimicrobial activity of MoS_2

and WS_2. WS_2 and MoS_2 were exfoliated and their antimicrobial activities were studied by changing the sonication time, solvent, and concentration of WS_2 and MoS_2 flakes. Accordingly, some of the methods and their antibacterial performances are discussed in the following sections.

Table 5.2. Range of ZOI corresponding to different susceptibility levels

≥ 15 mm	Susceptible (S)
11-14 mm	Intermediate (I)
≤ 10 mm	Resistant (R)
0 mm	No Zone (NZ)

Table 5.3. Susceptibility pattern of pathogens for few-layer WS_2 and MoS_2.

Nanostructures	Concentration (µg mL^{-1})	ZOI for *MS*	ZOI for *SA*	ZOI for *BC*	ZOI for *PA*	ZOI for *YP*	ZOI for *CA*
Few-layer MoS_2	~198	S	S	S	S	S	S
Few-layer WS_2	~610	I	S	S	S	S	S

Key: Intermediate= [I], Susceptible= [S]

5.4 Experimental details and antimicrobial assessment (Method 2)

5.4.1 Preparation of WS_2 and MoS_2 specimens

Using the same process described in method 1, exfoliation of WS_2 nanosheets was performed. However, this time, sonication was performed for 13 h.

5.4.2 Screening for antimicrobial activity

The pathogen viability when treated with exfoliated WS_2 is shown in **Fig. 5.9**. It is observed that for *MS* and *YP*, the activity is negligible. *PA* and *CA* are susceptible to these WS_2 nanostructures. However, *SA* and *BC* showed intermediate susceptibility.

5.5 Experimental details and antimicrobial assessment (Method 3)

5.5.1 Preparation of WS_2 and MoS_2 specimens

A mixture of isopropanol (IPA) (purchased from Merck®) and double distilled (DD) water was prepared in a ratio 1:4. The composition of the solution was taken based on the investigation done by Sajedi-Moghaddam *et al.* [30]. 1.6 mg of WS_2 and MoS_2 were then mixed with 1 mL of the mixture in separate beakers and ultra-sonicated for 6, 7, 8, 9 and 10 h in a bath sonicator (Jain Scientific Glass Works, output power 100 W) having output frequency 50 Hz. The temperature of the system was maintained below 30 °C. To avoid any accumulation of the WS_2 and MoS_2 flakes at the bottom of the container, the beakers were well shaken in every 10 min for the first one hour. After 6, 7, 8, 9, 10 h of sonication, TMDC specimens were collected and centrifuged for 1 hour at 2500 rpm and the supernatants were taken for antimicrobial analysis.

5.5.2 Screening for antimicrobial activity

It was observed that these specimens did not show antibacterial activity as ZOI was absent for all the specimens.

5.6 Experimental details and antimicrobial assessment (Method 4)

5.6.1 Preparation of WS_2 and MoS_2 specimens

A mixture of IPA and DD water was prepared in a ratio 1:4 as mentioned in method 3. Then, different amounts of WS_2 and MoS_2 flakes were put in the as-prepared mixture so that the concentrations become 500, 600, 700, 800, 900, and 1000 µg mL^{-1}. Then the mixtures were ultra-sonicated for 6 h. After 6 h of sonication, specimens were directly used for antimicrobial assessment without performing any further treatment on them. The specimens obtained are shown in **Fig. 5.10.**

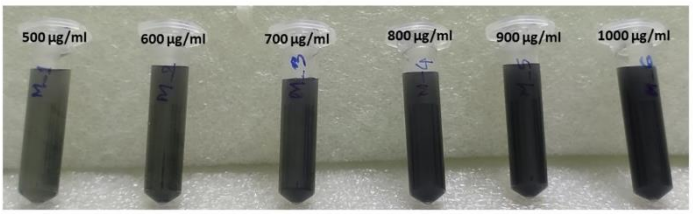

MoS_2 dispersed in IPA /H_2O

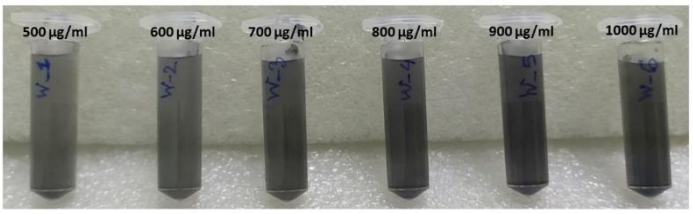

WS_2 dispersed in IPA/H_2O

Fig.5.10. Different concentrations of exfoliated MoS_2 and WS_2 in IPA-H_2O solvent after 6 h of exfoliation.

5.6.2 Screening for antimicrobial activity

In this case, antibacterial analysis was performed against *MS, SA, BC, PA, YP* and *E.Coli (EC)*. Here Gentamicin (G) is taken as the positive control for antibacterial assessment involving *MS, SA, BC, PA, YP* and *E.Coli (EC)*. It was observed that these WS_2 and MoS_2 specimens do not exhibit antimicrobial activity as no ZOI can be seen for all the specimens.

5.7 Discussions

5.7.1 Comparison of antimicrobial activities of WS_2 and MoS_2 specimens exfoliated through different methods.

Table 5.4. Susceptibility pattern of pathogens for WS_2 and MoS_2 specimens exfoliated through different methods.

Method		Concentration of WS_2 /MoS_2 (μg mL^{-1})	ZOI (*MS*)	ZOI (*SA*)	ZOI (*BC*)	ZOI (*PA*)	ZOI (*YP*)	ZOI (*CA*)	ZOI (*EC*)
1	MoS_2	~198	S	S	S	S	S	S	NA
	WS_2	~610	I	S	S	S	S	S	NA
2	MoS_2	NA	NA	NA	NA	NA	NA	NA	NA
	WS_2	~270	NZ	I	I	S	NZ	S	NA
3	MoS_2	~50	NZ	NZ	NZ	NZ	NZ	NZ	NA
	WS_2	~80	NZ	NZ	NZ	NZ	NZ	NZ	NA
4	MoS_2	500,600,700,800, 900 & 1000	NZ	NZ	NZ	NZ	NZ	NZ	NZ
	WS_2	500,600,700,800, 900 & 1000	NZ	NZ	NZ	NZ	NZ	NZ	NZ

Key: NZ= no zone, Intermediate= [I], Susceptible= [S], Not applicable [NA]

Table 5.4 compares the antimicrobial activities of WS_2 and MoS_2 specimens exfoliated through different methods. WS_2 and MoS_2 were exfoliated in NMP and IPA-H_2O in different ways, and their antimicrobial activities were studied by changing the sonication time, solvent, and concentration of the TMDC flakes. In, method 1, ultrasonication of WS_2 was performed for 10 h, while in method 2, it was performed for 13 h. However, it was observed that the results were moderate for the latter, which implies that an increase in sonication time may not increase antimicrobial activity. Again, the complete absence of ZOI was observed for WS_2 and MoS_2 exfoliated in an iso-propanol (IPA)-H_2O mixture and sonicated for different durations (method 3, **Table 5.4**). This result strengthens the conclusion made above that the antimicrobial properties do not directly

depend on the sonication time. We also tested the antimicrobial properties of highly poly-dispersed specimens (method 4, **Table 5.4**) in which high concentration of WS_2 and MoS_2 multi-layered nanostructures were there. However, the results were not at all significant. This implies that simply increasing the concentrations of MoS_2 and WS_2 specimens does not give rise to antimicrobial activity. From the discussion, it can be concluded that the antimicrobial activity of WS_2 and MoS_2 nanosheets does not directly depend on the sonication time or concentration of material particles present in the system.

5.7.2 Parameters responsible for antimicrobial activities of WS_2 and MoS_2 nanosheets

Yang *et al.* [22] investigated the antimicrobial activity of chemically exfoliated(ce) MoS_2 nanosheets (monolayer, thickness 1 nm, size ~ 200 nm), aggregated ce-MoS_2 nanosheets (thickness ~10 nm, size ~ 1–2 μm), and bulk nanosheets. They concluded that the antimicrobial activity depends on the morphology (shape and specific area) of the material. Navale *et al.* [19] prepared few-layered (1–5 nm thick, length ~1–3 μm) WS_2 nanosheets and concluded that antibacterial activity increased with increasing nanosheet concentration and incubation time. Pandit *et al.* [23] reported on the antibacterial activity of MoS_2 having single layer. Similarly, Liu *et al.* [20] also synthesized monolayer WS_2 using a surfactant exfoliation method and concluded that the antibacterial activity increased with increasing concentration and incubation time. These reports suggest that WS_2 and MoS_2 nanosheets show antimicrobial activity when the material specimen contains sufficient amount of monolayer and few-layer nanostructures.

In the present case, the TEM results reveal that the exfoliated sheets obtained through Method 1 exhibit a predominantly mono/few-layer nanostructures, a characteristic corroborated by the specimen photographs presented in **Fig. 5.2.** and specimen micrographs presented in **Fig.5.4**. Conversely, exfoliated sheets derived from Method 4 manifest a multilayer composition. Comparative analysis in **Table 5.4**. indicates that although the concentration of WS_2 and MoS_2 is higher in Method 4, no Zone of Inhibition (ZOI) is observed. This observation suggests that an increase in antibacterial activity corresponds with an increase in the concentration of monolayer/few-layer Transition Metal Dichalcogenides (TMDC).

5.7.3 Mechanism of antipathogenic activity

Few studies have reported the detailed anti-pathogenic mechanisms of MoS_2 and WS_2 against specific pathogens. As reported, for MoS_2 nanosheets, it is a multistep process. The embedment of the nanosheets into the cell body starts because of the electrostatic attraction between the cell membrane and nanosheets. Then, the nanosheets were further pulled into the body of the cell owing to the van der Waals force between the nanosheets and phospholipids present in the cell body. This process is followed by the extraction of phospholipid molecules [31]. In some cases, the process of embedding nanosheets on the bacterial cell and the extraction of phospholipids together causes rapid depolarization in the cell. Depolarization alters permeability across the membrane and initiates membrane disruption [24]. This process further inhibits the normal respiratory process and eventually the metabolic activity of bacteria. Bacterial death is accelerated by a simultaneous increase in oxidative stress [22, 23, 32]. On the other hand, as reported, for WS_2 nanosheets, the antimicrobial activity occurs mainly due to membrane destruction [19-20]. In the present context, it is observed that the MoS_2 and WS_2 nanosheets used for the antimicrobial activity are neutral, therefore in the current context, the antimicrobial mechanism is elucidated as follows: upon contact, nanomaterials engage microbial cells by interacting with phospholipids through van der Waals forces. The nanomaterial thickness is remarkably smaller, approximately 10^2-10^3 times, than the size of microbial cells, potentially inducing physical membrane disruption and consequential disturbance to essential cell components. **Table 5.5** compares the different antimicrobial studies on WS_2 and MoS_2 nanosheets and their composites.

Table 5.5. Comparison of different antimicrobial studies carried out on WS_2 and MoS_2 nanostructures and their composites

Material	**Concentration**	**Method of analysis**	**Pathogens**	**Incubation time**	**Ref**
WS_2	250 µg mL^{-1}	Colony counting method	*[1]EC, [2]ST, [3]BS, [4]SE*	6 h	[19]
r-GO-WS_2	250 µg mL^{-1}				
WS_2 nanosheets	200 µg mL^{-1}	Colony forming unit	*[1]EC, [5]SA*	2 h	[20]
WS_2/ZnO	300 µg mL^{-1}	Disc diffusion	*[6]CA*	NA	[21]

MoS_2 nanosheets	20 µg mL^-	Colony counting method	[7]*EC DH5α*	6 h	[22]
MoS_2 nanosheets Functionalized with thiol ligands	25.12 µg mL^{-1}	Microbroth dilution method	[5]*SA*, [8]*PA*	72 h	[23]
MoS_2 nanosheets		Colony counting method	*Salmonella wild-type Salmonella*	24 h	[24]
MoS_2 nanosheets	1000 µg mL^{-1}	metabolomics	[1]*EC*	12 h	[33]
Iron doped MoS_2 coated on titanium	100 µg mL^{-1}	Agar diffusion assay	[1]*EC*, [5]*SA*	24 h	[34]
MoS_2 nanostructures	NA	Agar method	[9]*AA*	NA	[35]
MoS_2 - modified curcumin nanostructures	50 µg mL^{-1}	Confocal analysis	[10]*KP*	18 h	[36]
Chitosan/Ag/ MoS_2	NA	Colony counting method	[5]*SA*,[1]*EC*	20 min	[37]
O, N co-doped MoS_2 nanoflowers	2 mg mL^{-1}	Triphenyl Tetrazolium Chloride assay	[9]*AA*, [11]*FO*	24 h	[38]
MoS_2	~ 198 µg mL^{-1} (MoS_2)	Agar well diffusion assay	[5]*SA*,[6]*CA*, [8]*PA*, [12]*PD*, [13]*MS* ,[14]*BC*, [15] *YP*	24 h	Present
WS_2	~610 µg mL^{-1} (WS_2)				

[1]*E.coli (EC),* [2]*S.typhimurium (ST),* [3]*B.subtilis (BS),* [4]*S.emidermidis (SE)*, [5]*S. aureus (SA)*, [6]*C. albicans (CA),* [7]*E.coli DH5α (EC DH5α)*, [8]*P.Aeruginosa (PA*), [9]*Alternaria alternata (AA),* [10]*Klebsiella pneumoniae (KP),* [11]*F. oxysporum (FO),*[12]*P. Diminuta*, & *M. Smegmatis (MS),* [14]*B. Cereus (BC),* [15] *Y. Pestis (YP)*

5.8 Conclusion

This chapter extensively deals with antimicrobial analysis of WS_2 and MoS_2 nanosheets exfoliated using different techniques. Antipathogenic analysis was performed using the agar well diffusion assay. The MoS_2 sample exfoliated in NMP for 4 h followed by liquid cascading centrifugation showed antimicrobial activity for all the microbes considered in the present investigation, viz- *M. smegmatis, S. aureus, B. cereus, P. aeruginosa, Y. pestis and C. albicans*. All the pathogens were susceptible to this sample. The concentration of few layers in this sample was approximately 198 µg mL^{-1}. Similarly, the WS_2 sample exfoliated in NMP for 10 h, followed by liquid cascading centrifugation, showed antimicrobial activity against all pathogens. *M. smegmatis* showed intermediate susceptibility to this sample, whereas all other pathogens were found to be fully susceptible to this specimen. The concentration of few layers in this sample was ~610 µg mL^{-1}. It was realized that, these materials show antimicrobial properties only when they have certain concentration of mono or few-layer nanostructures in the material system. It is realized that changes in exfoliation parameters will affect the antimicrobial activity only if they are able to increase the number of monolayers or few layers in the system. From the results, it can also be concluded that MoS_2 is more effective as antipathogenic agent than that of WS_2 few layer nanostructures; as synthesis of MoS_2 is two times less time consuming than that of WS_2 and the less amount of MoS_2 nanosheets can show enhanced antimicrobial activity than WS_2 nanosheets.

References

[1] Splendiani, A., Sun, L., Zhang, Y., Li, T., Kim, J., Chim, C.Y., Galli, G. and Wang, F. Emerging photoluminescence in monolayer MoS_2. *Nano Letters*, 10(4):1271-1275, 2010.

[2] Choi, W., Cho, M.Y., Konar, A., Lee, J.H., Cha, G.B., Hong, S.C., Kim, S., Kim, J., Jena, D., Joo, J. and Kim, S. High-detectivity multilayer MoS_2 phototransistors with spectral response from ultraviolet to infrared. *Advanced Materials*, 24(43):5832-583, 2012.

[3] Neog, A. and Biswas, R. Evidence of Laser-Induced Amplification of Random Noise in WS_2 Nanosheets Based Resistive System. *Physica Status Solidi (RRL)–Rapid Research Letters*, 16(8): 2200142, 2022.

[4] Xu, Y., Hsieh, C.Y., Wu, L. and Ang, L.K. Two-dimensional transition metal dichalcogenides mediated long range surface plasmon resonance biosensors. *Journal of Physics D: Applied Physics*, 52(6): 065101, 2018.

[5] Monga, D., Sharma, S., Shetti, N.P., Basu, S., Reddy, K.R. and Aminabhavi, T.M. Advances in transition metal dichalcogenide-based two-dimensional nanomaterials. *Materials Today Chemistry*,19:100399, 2021.

[6] Neog, A. and Biswas, R. WS_2 nanosheets as a potential candidate towards sensing heavy metal ions: A new dimension of 2D materials. *Materials Research Bulletin*, 144: 111471, 2021.

[7] Neog, A. and Biswas, R. A novel route for sensing heavy metal ion in aqueous solution. *Europhysics Letters*, 139: 46002, 2022

[8] Liao, W., Zhao, S., Li, F., Wang, C., Ge, Y., Wang, H., Wang, S. and Zhang, H. Interface engineering of two-dimensional transition metal dichalcogenides towards next-generation electronic devices: recent advances and challenges. *Nanoscale Horizons*, 5(5): 787-807, 2020.

[9] Zeng, H., Dai, J., Yao, W., Xiao, D. and Cui, X. Valley polarization in MoS_2 monolayers by optical pumping. *Nature Nanotechnology*, 7(8): 490-493, 2012.

[10] Cao, T., Wang, G., Han, W., Ye, H., Zhu, C., Shi, J., Niu, Q., Tan, P., Wang, E., Liu, B. and Feng, J. Valley-selective circular dichroism of monolayer molybdenum disulphide. *Nature Communications*, 3(1): 1-5, 2012.

[11] Ramasubramaniam, A., Naveh, D. and Towe, E. Tunable band gaps in bilayer transition-metal dichalcogenides. *Physical Review B*, 84(20): 205325, 2011.

[12] Zhao, Y., Liu, J., Zhang, X., Wang, C., Zhao, X., Li, J. and Jin, H. Convenient Synthesis of WS_2–MoS_2 Heterostructures with Enhanced Photocatalytic Performance. *The Journal of Physical Chemistry C*, 123(45): 27363,2019.

[13] Kibsgaard, J., Chen, Z., Reinecke, B.N. and Jaramillo, T.F. Engineering the surface structure of MoS_2 to preferentially expose active edge sites for electrocatalysis. *Nature Materials*, 11(11): 963-969, 2012.

[14] Zhang, X., Teng, S.Y., Loy, A.C.M., How, B.S., Leong, W.D. and Tao, X. Transition metal dichalcogenides for the application of pollution reduction: A review. *Nanomaterials*, 10(6): 1012, 2020.

[15] Redlich, M., Katz, A., Rapoport, L., Wagner, H.D., Feldman, Y. and Tenne, R. Improved orthodontic stainless-steel wires coated with inorganic fullerene-like nanoparticles of WS_2 impregnated in electroless nickel–phosphorous film. *Dental Materials*, 24(12):1640-1646 , 2008.

[16] Wu, H., Yang, R., Song, B., Han, Q., Li, J., Zhang, Y., Fang, Y., Tenne, R. and Wang, C. Biocompatible inorganic fullerene-like molybdenum disulfide nanoparticles produced by pulsed laser ablation in water. *ACS Nano*, 5(2): 1276-1281, 2011.

[17] Teo, W.Z., Chng, E.L.K., Sofer, Z. and Pumera, M. Cytotoxicity of exfoliated transition-metal dichalcogenides (MoS_2, WS_2, and WSe_2) is lower than that of graphene and its analogues. *Chemistry–A European Journal*, 20(31): 9627-9632, 2014.

[18] Appel, J.H., Li, D.O., Podlevsky, J.D., Debnath, A., Green, A.A., Wang, Q.H. and Chae, J. Low cytotoxicity and genotoxicity of two-dimensional MoS_2 and WS_2. *ACS Biomaterials Science & Engineering*, 2(3): 361-367, 2016.

[19] Navale, G.R., Rout, C.S., Gohil, K.N., Dharne, M.S., Late, D.J. and Shinde, S.S. Oxidative and membrane stress-mediated antibacterial activity of WS_2 and rGO-WS_2 nanosheets. *Rsc Advances*, 5(91): 74726-74733, 2015.

[20] Liu, X., Duan, G., Li, W., Zhou, Z. and Zhou, R. Membrane destruction-mediated antibacterial activity of tungsten disulfide (WS_2). *Rsc Advances*, 7(60):37873-37880, 2017.

[21] Bhatt, V.K., Patel, M., Pataniya, P.M., Iyer, B.D., Sumesh, C.K. and Late, D.J. Enhanced antifungal activity of WS_2/ZnO nanohybrid against Candida albicans. *ACS Biomaterials Science & Engineering*, 6(11):6069-6075, 2020.

[22] Yang, X., Li, J., Liang, T., Ma, C., Zhang, Y., Chen, H., Hanagata, N., Su, H. and Xu, M. Antibacterial activity of two-dimensional MoS_2 sheets. *Nanoscale*, 6(17):10126-10133, 2014.

[23] Pandit, S., Karunakaran, S., Boda, S.K., Basu, B. and De, M. High antibacterial activity of functionalized chemically exfoliated MoS_2. *ACS Applied Materials & Interfaces*, 8(46):31567-31573, 2016.

[24] Kaur, J., Singh, M., Dell'Aversana, C., Benedetti, R., Giardina, P., Rossi, M., Valadan, M., Vergara, A., Cutarelli, A., Montone, A.M.I. and Altucci, L. Biological interactions of biocompatible and water-dispersed MoS_2 nanosheets with bacteria and human cells. *Scientific Reports*, 8(1):1-15, 2018.

[25] Backes, C., Szydłowska, B.M., Harvey, A., Yuan, S., Vega-Mayoral, V., Davies, B.R., Zhao, P.L., Hanlon, D., Santos, E.J., Katsnelson, M.I. and Blau, W.J. Production of highly monolayer enriched dispersions of liquid-exfoliated nanosheets by liquid cascade centrifugation. *ACS Nano*, 10(1):1589-1601, 2016.

[26] Gamazo, C., Prior, S., Concepción Lecároz, M., Vitas, A.I., Campanero, M.A., Pérez, G., Gonzalez, D. and Blanco-Prieto, M.J. Biodegradable gentamicin delivery systems for parenteral use for the treatment of intracellular bacterial infections. *Expert Opinion on Drug Delivery*, 4(6): 677-688, 2007.

[27] Park, N.H. and Kang, M.K. Antifungal and antiviral agents. *Pharmacology and Therapeutics for Dentistry*, 5: 660-6, 2004.

[28] Neog, A., Deb, S. and Biswas, R. Atypical electrical behavior of few layered WS_2 nanosheets based platform subject to heavy metal ion treatment. *Materials Letters*, 268:127597, 2020.

[29] Hayat, A. and Munnawar, F. Antibacterial effectiveness of commercially available hand sanitizers. *Int J Biol Biotech*, 13(3):427-431, 2016.

[30] Sajedi-Moghaddam, A. and Saievar-Iranizad, E. High-yield exfoliation of tungsten disulphide nanosheets by rational mixing of low-boiling-point solvents. *Materials Research Express*, 5(1): 015045, 2018.

[31] Gu, Z., Li, W., Hong, L. and Zhou, R. Exploring biological effects of MoS_2 nanosheets on native structures of α-helical peptides. *The Journal of Chemical Physics*, 144(17):175103, 2016.

[32] Roy, S., Mondal, A., Yadav, V., Sarkar, A., Banerjee, R., Sanpui, P. and Jaiswal, A. Mechanistic insight into the antibacterial activity of chitosan exfoliated MoS_2 nanosheets: membrane damage, metabolic inactivation, and oxidative stress. *ACS Applied Bio Materials,*2(7): 2738-2755, 2019.

[33] Wu, N., Yu, Y., Li, T., Ji, X., Jiang, L., Zong, J. and Huang, H. Investigating the influence of MoS_2 nanosheets on E. coli from metabolomics level. *PloS one*, 11(12): e0167245, 2016.

[34] Tang, K., Wang, L., Geng, H., Qiu, J., Cao, H. and Liu, X. Molybdenum disulfide (MoS_2) nanosheets vertically coated on titanium for disinfection in the dark. *Arabian Journal of Chemistry*, 13(1): 1612-1623, 2020.

[35] Basu, P., Chakraborty, J., Ganguli, N., Mukherjee, K., Acharya, K., Satpati, B., Khamrui, S., Mandal, S., Banerjee, D., Goswami, D. and Nambissan, P.M. Defect-engineered MoS_2 nanostructures for reactive oxygen species generation in the dark: antipollutant and antifungal performances. *ACS Applied Materials & Interfaces*, 11(51): 48179-48191, 2019.

[36] Singh, A.K., Mishra, H., Firdaus, Z., Yadav, S., Aditi, P., Nandy, N., Sharma, K., Bose, P., Pandey, A.K., Chauhan, B.S. and Neogi, K. MoS_2-modified curcumin nanostructures: the novel theranostic hybrid having potent antibacterial and antibiofilm activities against multidrug-resistant hypervirulent klebsiella pneumoniae. *Chemical Research in Toxicology*, 32(8): 1599-1618, 2019.

[37] Zhu, M., Liu, X., Tan, L., Cui, Z., Liang, Y., Li, Z., Yeung, K.W.K. and Wu, S. Photo-responsive chitosan/Ag/MoS_2 for rapid bacteria-killing. *Journal of Hazardous Materials*, 383: 121122, 2020.

[38] Basu, P., Mukherjee, K., Khamrui, S., Mukherjee, S., Ahmed, M., Acharya, K., Banerjee, D., Nambissan, P.M. and Chatterjee, K. Oxygen, nitrogen co-doped molybdenum disulphide nanoflowers for an excellent antifungal activity. *Materials Advances*, 1(6): 1726-1738, 2020.